Convolutional modeling of diffraction effects in pulse-echo ultrasound imaging

T. Douglas Mast
Department of Biomedical Engineering, University of Cincinnati, Cincinnati, Ohio 45267
doug.mast@uc.edu

Abstract: A model is presented for pulse-echo imaging of three-dimensional, linear, weakly-scattering continuum media by ultrasound array transducers. The model accounts for the diffracted fields of focused array subapertures in both transmit and receive modes, multiple transmit and receive focal zones, frequency-dependent attenuation, and aberration caused by mismatched medium and beamformer sound speeds. For a given medium reflectivity function, computation of a B-scan requires evaluation of a depth-dependent transmit/receive beam product, followed by two one-dimensional convolutions and a one-dimensional summation. Numerical results obtained using analytic expressions for transmit and receive beams agree favorably with measured B-scan images and speckle statistics.

PACS numbers: 43.80.Vj, 43.20.El, 43.20.Fn [CC]
Date Received: March 22, 2010 **Date Accepted:** June 4, 2010

1. Introduction

Pulse-echo ultrasound imaging is a ubiquitous modality employed in medicine. Typically, an ultrasound array transducer transmits pulsed waves into an inhomogeneous scattering medium and receives backscattered acoustic pressure signals, which are then electronically beamformed. The resulting spatial map of echo brightness, or B-scan, can be considered an image of position-dependent reflectivity or scattering strength in the inhomogeneous medium.

Several previous methods for simulation of B-scan imaging have been based on convolution of a computed or measured point-spread function with a collection of point scatterers.[1] This simple convolution approach has been extended to include depth-dependent variations in the system point-spread function,[2] but still does not fully represent aperture diffraction effects. Other approaches have incorporated more realistic propagation, scattering, and beamforming of ultrasound fields, computed by numerical integration and summation under the Fresnel approximation[3] or the impulse-response approach.[4] Although these methods are successful at depicting diffraction effects, they are computationally intensive for B-scan imaging of three-dimensional media containing a realistic number of scattering sites.

The model presented here aims to accurately depict aperture diffraction effects and scattering from a continuous tissue medium while maintaining the high efficiency of convolution-based models. This analysis leads to a simple computational method that simulates B-scan or other pulse-echo image data, given a three-dimensional tissue model and computed transmit and receive beam patterns. This method, which requires only numerical evaluation of two one-dimensional convolutions and a single one-dimensional integration, is tested by simulating B-scans of a standard ultrasound quality assurance phantom by a typical linear array imaging system. Accuracy of the simulated image data is assessed by comparison with measurements from the system configuration simulated.

2. Theory

The configuration modeled here is geometrically sketched in Fig. 1. A portion of an ultrasound array, taken without loss of generality to be centered at the origin, is modeled as a radiator within an infinite rigid baffle in the plane $\mathbf{r}_s=(x_s,y_s,0)$, with normal velocity $v(x_s,y_s,t)=v_0A(x_s,y_s)w(t)e^{-i\omega t}$. A receiving aperture centered at the same position then detects

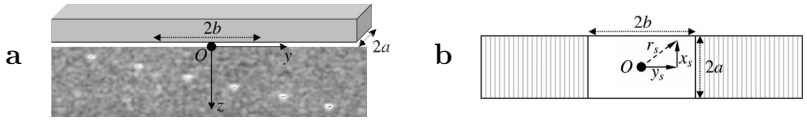

Fig. 1. Configuration for B-scan simulations. (a) Schematic of transducer array with active width $2a$ in the x (elevation, or out-of-plane) direction and active subaperture width $2b$ in the y (azimuthal) direction. Position vectors in the inhomogeneous medium are $\mathbf{r}_0=(x_0,y_0,z_0)$ for the variable of integration and $\mathbf{r}=(0,y,z)$ for position in the B-scan image. (b) Schematic of the transducer surface (perpendicular to (a), showing the origin, subaperture widths, and position vector $\mathbf{r}_s=(x_s,y_s,0)$ in the active plane.

the scattered pressure field, assumed to emanate from a three-dimensional, linear, lossy, weakly inhomogeneous medium. For a slowly-varying pulse envelope $w(t)$, the backscattered pressure at a point $\mathbf{r}_s$ on the receiving aperture surface is then[5,6]

$$p_s(\mathbf{r}_s,t)=\frac{k^2e^{-i\omega t}}{4\pi}\int_{V_0}w\left(t-\frac{|\mathbf{r}_0-\mathbf{r}_s|-r_0}{c}\right)\gamma(\mathbf{r}_0)p_E(\mathbf{r}_0)\frac{e^{ik|\mathbf{r}_0-\mathbf{r}_s|}}{|\mathbf{r}_0-\mathbf{r}_s|}dV_0, \tag{1}$$

where ω is the radial center frequency of the velocity pulse, c is the speed of sound, $k=\omega/c$ is the corresponding wavenumber, $\gamma=\gamma_\kappa-\gamma_\rho$ is the medium reflectivity dependent on local compressibility and density variations γ_κ and γ_ρ,[5] and p_E is the pressure emitted by the radiating aperture for a time-harmonic source velocity,

$$p_E(\mathbf{r}_0)=-\frac{ik\rho cv_0}{2\pi}\int_{-\infty}^{\infty}\int_{-\infty}^{\infty}A_E(x_s,y_s)\frac{e^{ik_0|\mathbf{r}_0-\mathbf{r}_s|}}{|\mathbf{r}_0-\mathbf{r}_s|}dx_sdy_s, \tag{2}$$

where $v_0A_E(x_s,y_s)$ is the amplitude of the normal velocity at an emitting point $\mathbf{r}_s=(x_s,y_s)$ on the radiator surface. The signal recorded by the receiving aperture centered at $y=0$ is then

$$u(t)=\int_{-\infty}^{\infty}\int_{-\infty}^{\infty}A_D(x_s,y_s)p_s(\mathbf{r}_s,t)dx_sdy_s, \tag{3}$$

where A_D is the relative detector sensitivity at a point $\mathbf{r}_s$ on the receiving aperture.

For the typical case of focused transmit and receive apertures, the largest contributions to the received signal $u(t)$ result from scattering sites near the axis $(x_0,y_0)=(0,0)$. Thus, the pulse envelope appearing in Eq. (1) can be approximated as

$$w\left(t-\frac{r_0}{c}-\frac{|\mathbf{r}_s-\mathbf{r}_0|}{c}\right)\approx w\left(t-\frac{2z_0}{c}\right). \tag{4}$$

Making this approximation and combining Eqs. (1)–(3) yields the received signal

$$u(t)=\frac{ike^{-i\omega t}}{2\rho cv_0}\int_{V_0}w\left(t-\frac{2z_0}{c}\right)\gamma(\mathbf{r}_0)p_E(\mathbf{r}_0)p_D(\mathbf{r}_0)dV_0, \tag{5}$$

which constitutes the analytic, radiofrequency (RF) A-line recorded by transmit and receive apertures centered at the origin. In Eq. (5), the detector beam p_D is defined in analogy to the emitter beam defined by Eq. (2).

The complex transmit-receive beam product appearing in Eq. (5) is now written as a "system function,"[6]

$$\Lambda(x_0,y_0,z_0)=p_E(\mathbf{r}_0)p_D(\mathbf{r}_0). \tag{6}$$

A pulse-echo image pixel at the position (y,z) is then defined as an instantaneous value of the analytic RF signal recorded by transmit and receive apertures centered at $(0,y,0)$ in the source plane,

$$I(y,z) = \left[u\left(\frac{2z}{c}\right) \right]_{(0,y,0)}$$
$$= \frac{ike^{-i\omega t}}{2\rho c v_0} \int_{z_0} w\left(\frac{2(z-z_0)}{c}\right) \int_{x_0} \left[\int_{y_0} \gamma(\mathbf{r}_0)\Lambda(x_0, y_0 - y, z_0) dy_0 \right] dx_0 dz_0$$
$$= \frac{ike^{-i\omega t}}{2\rho c v_0} w\left(\frac{2z}{c}\right) \otimes_z \int_x \gamma(\mathbf{r}) \otimes_y \Lambda(\mathbf{r}) dx, \quad (7)$$

where the symbols $\otimes_y$ and $\otimes_z$ represent one-dimensional convolutions along their respective directions.

In the approach summarized by Eq. (7), simulation of a B-scan image consists of the following computational steps:

1. Convolve the medium reflectivity function $\gamma(\mathbf{r})$ with the complex emitter-detector beam product $\Lambda(\mathbf{r})$ along the array direction y.
2. Integrate this convolution product along the elevation direction x.
3. Convolve this integral result with the pulse envelope $w(2z/c)$ along the range direction z.

As demonstrated below, this simulation method can be efficiently implemented by computing the beam product $\Lambda(\mathbf{r})$ using a Fresnel approximation[7] and evaluating the one-dimensional convolutions of Eq. (7) using fast Fourier transforms.

3. Simulations

The image model summarized by Eq. (7) was tested using B-scan images and speckle statistics measured using a 7 MHz, 192-element linear array transducer (L7) controlled by the Iris 2 imaging platform (Ardent Sound, Mesa, Arizona). The medium imaged was a standard reference phantom (Model 539, ATS Laboratories, Bridgeport, Connecticut), consisting of a polyurethane background medium (sound speed 1.454 mm/μs and attenuation of 0.499 dB/cm/MHz [5.76×10^{-3} Np/mm/MHz] from manufacturer measurements) with randomly placed scatterers, nylon wire targets, and scatterer-free (cyst) targets. Beamformed RF A-line signals were acquired at 33 MHz by a 14-bit A/D card (Compuscope CS14200, Gage Applied, Montreal, Canada). To reduce electronic and discretization noise, RF A-lines from 52 frames were averaged coherently. A-lines were then filtered by a bandpass filter with −6 dB points 1.8 and 9.3 MHz, their analytic envelopes were computed by Hilbert transformation, and B-scans were displayed as the log-scaled envelope magnitude.

Simulations were performed using MATLAB 7.4 (The MathWorks, Natick, MA). Simulation parameters were configured to match the above imaging configuration as closely as possible, including a transducer elevation width of 7.0 mm, 192 A-lines separated by a pitch of 0.22 mm, depth-dependent transmit and receive apertures with sizes, azimuthal focal lengths, and gain factors matching the dynamic focusing performed by the Iris 2 system, and the Gaussian transmit pulse $w(t)e^{-i\omega t} = e^{-t^2/(2\sigma^2)}e^{-i2\pi f_0 t}$ with a length parameter $\sigma = 0.25$ μs and an initial center frequency $f_0 = 6.1$ MHz. Effects of frequency-dependent attenuation on both pulse center frequency[8] and beam amplitude were represented by the depth-dependent wave number

$$k(z) = 2\pi \frac{f_0 - \alpha_0 z/(2\pi^2\sigma^2)}{c} + i\alpha_0 f_0, \quad (8)$$

where α_0 is the medium attenuation in Np/mm/MHz.

The medium reflectivity $\gamma(\mathbf{r})$ was specified on a $66 \times 228 \times 1573$ grid spanning 14.5 mm in the elevation direction ($\Delta x = 0.22$ mm), 50.2 mm in the azimuth direction ($\Delta y = 0.22$ mm), and 62.9 in the elevation direction ($\Delta z = 0.04$ mm, corresponding to a temporal sampling rate of 18.2 MHz). The randomly-scattering background was modeled

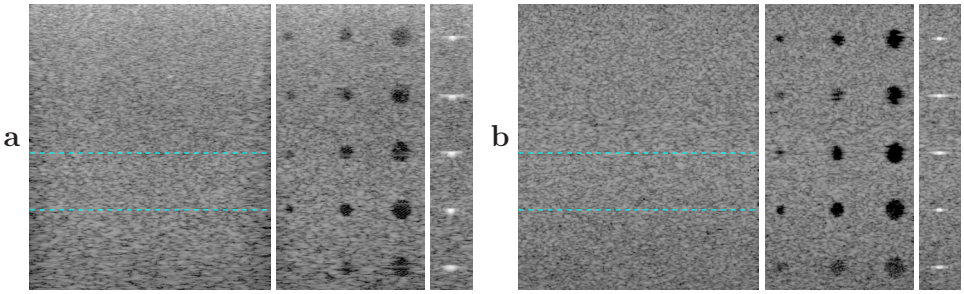

Fig. 2. (Color online) B-scans of the ATS 539 phantom. From left to right, each panel shows images of speckle (with the region of interest for statistical calculations indicated by dashed lines), scatterer-free cysts of diameter 2–4 mm at depths of 10–50 mm, and wire targets of diameter 0.1 mm at depths of 10–50 mm. Each B-scan is shown with a total depth of 50 mm on a logarithmic gray scale with 60 dB dynamic range. (a) Measurement. (b) Simulation.

by Gaussian white noise with rms reflectivity amplitude 1.6×10^{-2} over the region ($|x|<7.25$ mm, $|y|<21.2$ mm, $z<61$ mm). Wire targets were defined over the same region as single-pixel cylinders of amplitude 1, while cystic targets were defined as homogeneous ($\gamma=0$) cylindrical regions of radii 2–4 mm, each at locations to match the ATS 539 phantom.

To obtain B-scan images, the system function $\Lambda(\mathbf{r})$ was computed using the Fresnel approximation.[7] This approach provides analytic, approximate solutions of Eq. (2) for rectangularly symmetric sources, including separate azimuth and elevation focusing as well as a variety of transducer apodizations. The present simulations approximated each multiple-element transmit or receive aperture by a rectangular aperture of equal size. Focus aberration, caused in electronically-focused imaging systems by errors in the assumed sound speed, was incorporated by employing the system-assumed sound speed in computation of focal delays, while the true medium sound speed was used for all propagation calculations.

Subaperture sizes $2a\times2b$ were chosen to match the depth-dependent apertures employed by the Iris 2 system. Edge effects were reduced using error-function apodization[7] with thickness parameters $\sigma_x=\sigma_y=0.35$ mm. The transmit beam p_E was computed using a fixed azimuthal (y) focus at depth 36 mm, while the receive beam p_D was computed with depth-dependent azimuthal focusing at 14 focal depths between 2.6 and 63.7 mm. Computation time was conserved by computing $\Lambda(\mathbf{r})$ only within a single quadrant ($0<x<7.25$ mm, $0<y<4.0$ mm), including all points within −60 dB of the system function peak, and reproducing the other three quadrants by symmetry.

The three-step procedure of Eq. (7) was then implemented directly, with the x integration performed by discrete summation and the y and z convolutions performed by fast Fourier transforms. These one-dimensional convolution and integration operations yielded a complex B-scan image of the region ($|y|<21.1$ mm, $0<z<61$ mm). Electronic noise was simulated by adding Hilbert-transformed Gaussian random noise with an rms amplitude 85 dB below the maximum displayed brightness value. Depth-dependent gain compensation was then applied by multiplying the complex image data by the exponential factor $e^{\alpha_1 f_0 z}$, with $\alpha_1=5.19\times10^{-3}$ Np/mm/MHz. Computation time for one B-scan simulation, including calculation of the system function Λ and the image construction method of Eq. (7), was 45 s when implemented on a MATLAB 7.4 interpreter and run on a 2 GHz Intel Core 2 Duo processor with 3 Gbyte RAM under Mac OS X 10.4.11. This can be compared to computation times of many hours for comparable transducer configurations and 3D grid sizes using impulse-response based methods.[4]

Representative simulated B-scan images are compared to corresponding measured images of the ATS 539 phantom in Fig. 2. The overall depth-dependent speckle texture, point resolution, and contrast resolution of the two images show good agreement, with highest resolution near the transmit focal depth of 36 mm. Both images also show comparable degradation of resolution for the wire scatterers, due to sound speed mismatch (system-assumed sound

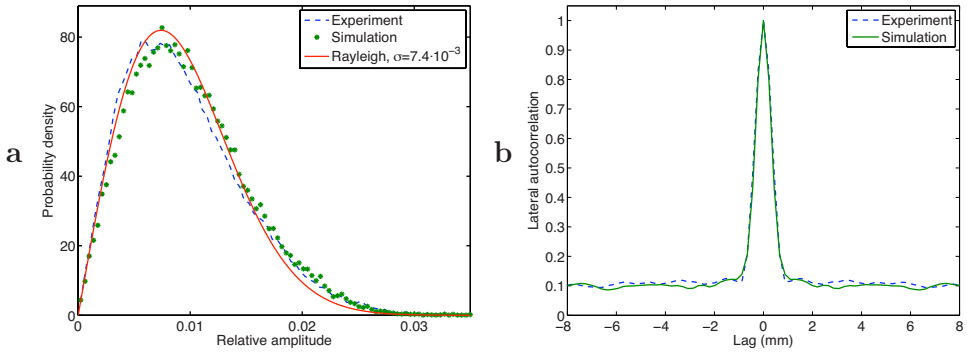

Fig. 3. (Color online) Statistics for measured and simulated speckle amplitude within the marked region of interest in Fig. 2. (a) Probability density functions estimated from 100-bin histograms of image amplitude, with Rayleigh distribution best fitting the measured histogram. (b) Azimuthal autocorrelation functions.

speed 1.540 mm/μs, actual sound speed 1.454 mm/μs). Features not accurately simulated include the depth asymmetry of the wire targets, as well as increased nearfield clutter due to ringdown of the transmit pulse.

Representative image statistics are shown in Fig. 3. Estimated probability density functions for the image amplitude $|I(y,z)|$ (expected to approach a Rayleigh distribution in the limit of fully-developed speckle) are shown for the depth range $30<z<40$ mm. Best-fitting parameters β of the Rayleigh probability distribution $P=\xi e^{-\xi^2/(2\beta^2)}/\beta^2$ are 7.4×10^{-3} for the measured image and 7.8×10^{-3} for the simulated image. Also shown are autocorrelation functions for the complex image $I(y,z)$ computed along the azimuthal (y) direction and averaged for all image rows within the same depth range. Half-maximum correlation lengths, corresponding to characteristic azimuthal speckle length scales (associated primarily with aperture-dependent diffraction effects) are 0.43 mm for the measured image and 0.40 mm for the simulated image. This agreement, as well as the overall similarity of depth-dependent speckle patterns seen in Fig. 2, suggests that diffraction effects on image texture have been successfully simulated by the present approach.

4. Discussion

The convolutional method presented here can be implemented for many different imaging configurations by appropriately modifying the system function $\Lambda(\mathbf{r})$. The Fresnel approximation for rectangularly symmetric elements can be applied to many additional transmit and receive focus characteristics and apodizations.[7] More complex imaging configurations, e.g., in which the transmit-receive beam product Λ varies with azimuthal position or the pulse envelope w varies with depth, can be simulated by computing Eq. (7) separately for each instance of these convolution kernels. Arbitrary multiple-element apertures with time-delay-based beamforming can be straightforwardly incorporated by superposition. System functions for arbitrary transmit and receive configurations can also be measured directly, or computed numerically by any available method.

The methods presented here, which simulate realistic B-scans for given transducer and scattering medium configurations, may be useful for any application requiring rapid computation of many pulse-echo images. This includes optimization of array and beamforming designs, for which a sequence of many images can be computed for a range of frequencies, aperture sizes, focal lengths, or other imaging system parameters, while holding the scattering medium constant.

Conversely, images of variable scattering media can be computed while holding system parameters constant. Such computations can be made very efficient by storing the system function $\Lambda(\mathbf{r})$ rather than recomputing it for each realization of the medium. Simulated images

can be made for media undergoing simulated motion, strain, or structural changes, or for multiple tissue volumes modeled from 3D histologic or computed tomography[9] maps of tissue structure.

The same approach laid out by Eq. (7) can also be applied to other imaging configurations, including passive imaging as used for spatially-sensitive passive cavitation detection.[10] In this approach, emissions from cavitating microbubbles or other acoustic sources are beam-formed by the same methods used for receive focusing in pulse-echo imaging, so that the only substantial difference from the procedure described above is the absence of a transmitted pulse. Thus, passive images can be directly simulated by Eq. (7) for the special case $w(t)=1$, $\Lambda(\mathbf{r})=p_D(\mathbf{r})$. Similarly, since the approach outlined here directly simulates beam-formed RF echo signals, its results can be applied to models of C-scan, integrated backscatter, or other pulse-echo imaging methods. The simple convolutional formulation of Eq. (7) may also be useful for analytic study of diffraction effects in pulse-echo imaging.

Acknowledgments

This work was supported by NIH grants R21 EB008483 and R43 CA124283.

References and links

[1]J. C. Bamber and R. J. Dickinson, "Ultrasonic B-scanning: A computer simulation," Phys. Med. Biol. **25**, 463–479 (1980).
[2]R. L. Maurice, G. Cloutier, J. Ohayon, and G. Finet, "Adapting the Lagrangian speckle model estimator for endovascular elastography: Theory and validation with simulated radio-frequency data," J. Acoust. Soc. Am. **116**, 1276–1286 (2004).
[3]Y. Li and J. A. Zagzebski, "A frequency domain model for generating B-mode images with array transducers," IEEE Trans. Ultrason. Ferroelectr. Freq. Control **46**, 690–699 (1999).
[4]J. A. Jensen and S. I. Nikolov, "Fast simulation of ultrasound images," Proc.-IEEE Ultrason. Symp. **2**, 1721–1724 (2000).
[5]P. M. Morse and K. U. Ingard, *Theoretical Acoustics* (McGraw-Hill, New York, 1968), Chap. 8.
[6]T. T. Jansson, T. D. Mast, and R. C. Waag, "Measurements of differential scattering cross- section using a ring transducer," J. Acoust. Soc. Am. **103**, 3169–3179 (1998).
[7]T. D. Mast, "Fresnel approximations for ultrasonic fields of rectangularly symmetric sources," J. Acoust. Soc. Am. **121**, 3311–3322 (2007).
[8]P. A. Narayana and J. Ophir, "A closed form method for the measurement of attenuation in nonlinearly dispersive media," Ultrason. Imaging **5**, 17–21 (1983).
[9]T. D. Mast, "Two- and three-dimensional simulations of ultrasonic propagation through human breast tissue," ARLO **3**, 53–58 (2002).
[10]V. A. Salgaonkar, S. Datta, C. K. Holland, and T. D. Mast, "Passive cavitation imaging with ultrasound arrays," J. Acoust. Soc. Am. **126**, 3071–3083 (2009).